

# Optimizing Differential Identifiability Improves Connectome Predictive Modeling of Cognitive Deficits in Alzheimer's Disease

Diana O. Svaldi PhD<sup>1\*</sup>, Joaquín Goñi PhD<sup>2,3,4</sup>, Kausar Abbas PhD<sup>2,3</sup>, Enrico Amico PhD<sup>2,3</sup>, David G. Clark<sup>1</sup>, Charanya Muralidharan<sup>1</sup>, Mario Dzemidzic PhD<sup>1</sup>, John D. West MS<sup>1</sup>, Shannon L. Risacher PhD<sup>1</sup>, Andrew J. Saykin PsyD<sup>1</sup>, Liana G. Apostolova MD, MSc<sup>1</sup>, for the Alzheimer's Disease Neuroimaging Initiative

<sup>1</sup> Indiana University School of Medicine, Indianapolis, IN, USA

<sup>2</sup> School of Industrial Engineering, Purdue University, West-Lafayette, IN, USA

<sup>3</sup> Purdue Institute for Integrative Neuroscience, Purdue University, West-Lafayette, IN, USA

<sup>4</sup> Weldon School of Biomedical Engineering, Purdue University, West-Lafayette, IN, USA

\* **corresponding author:** Diana O. Svaldi PhD, [dosvaldi@iu.edu](mailto:dosvaldi@iu.edu)

## Highlights

- Differential identifiability framework improves individual fingerprint in functional connectomes from individuals spanning the Alzheimer's disease spectrum
- Improved fingerprint leads to more stable and more precise identification of functional networks associated to cognitive deficits associated with Alzheimer's disease
- Improved fingerprint leads to improved accuracy and generalizability of individual level prediction of cognitive deficits from functional connectomes
- Default network and Frontoparietal networks are associated to a variety of cognitive deficits in Alzheimer's disease
- Dorsal Attention Network interactions with the Frontoparietal network are associated to cognitive tests with large attention components
- Visual network interacts with several networks in the brain in cognitive tests requiring imagery and semantic organization

## Abstract

Functional connectivity, as estimated using resting state fMRI, has shown potential in bridging the gap between pathophysiology and cognition. However, clinical use of functional connectivity biomarkers is impeded by unreliable estimates of individual functional connectomes and lack of generalizability of models predicting cognitive outcomes from connectivity. To address these issues, we combine the frameworks of connectome predictive modeling and differential identifiability. Using the combined framework, we show that enhancing the individual fingerprint of resting state functional connectomes leads to robust identification of functional networks associated to cognitive outcomes and also improves prediction of cognitive outcomes from functional connectomes. Using a comprehensive spectrum of cognitive outcomes associated to Alzheimer's disease, we identify and characterize functional networks associated to specific cognitive deficits exhibited in Alzheimer's disease. This combined framework is an important step in making individual level predictions of cognition from resting state functional connectomes and in understanding the relationship between cognition and connectivity.

**Keywords:** Alzheimer's Disease, cognition, resting state fMRI, functional connectivity, functional fingerprinting, predictive modeling

## 1 Introduction

The biological underpinnings of disorders characterized by cognitive or behavioral symptomatology remain poorly understood, contributing significantly to the bottleneck in treating these disorders [1]. In recent years, the application of complex systems analysis approaches for understanding how neural activity facilitates cognition has led to significant strides in characterizing these disorders. One such approach, functional brain connectomics, models functional brain networks as statistical dependencies in regional neural activity,

providing a framework to assess brain integration, segregation, and communication [2]. At the same time, the advent of resting state fMRI has allowed for in-vivo characterization of whole brain functional connectomes (FC) in humans [2], leading to the discovery of several critical brain networks implicated in schizophrenia, ADHD, autism, and Alzheimer's disease (AD) [3].

Despite their utility in understanding neurologic disorders, FC approaches have not yet been used translationally in the treatment of cognitive and behavioral disorders [4, 5]. To advance the treatment of such disorders, there is a critical need [5] to develop clinical biomarkers that are (1) robustly modulated by disease mechanisms and (2) specifically associated with disease related outcomes. Though FC has shown potential in bridging the gap between pathophysiology and cognition, its clinical use is impeded by unreliable estimation of individual level FC [6] and lack of generalizability of models predicting individual cognitive outcomes from FC [5]. Here we show that improving the subject level fingerprint of resting-state FC also improves prediction of cognitive deficits in AD. We also identify functional networks associated to specific cognitive deficits exhibited in AD.

## 1.1 Towards Improving Clinical Utility of FC

While FC shows differential group level associations across cognitive outcomes [7, 8] and across disease conditions [3, 9-13], it falls short of predicting clinically meaningful outcomes at the individual level. To address this, recent efforts in measuring FC fingerprinting at the individual level have shown that individuals can be reasonably distinguished from each other using FC as measured by identification rate [8, 14, 15] or differential identifiability [8]. Furthermore, recent studies have shown that individual level fingerprinting can be improved by brain state manipulation [14] or using data driven denoising methods [8]. Additionally, to improve the clinical utility of FC, efforts to improve individual prediction of cognition and behavior have been developed [4, 5, 16-18]. Among frameworks that use FC to predict individual differences in behavior or cognition, connectome predictive modeling (CPM) is the most used [16]. The CPM pipeline involves: (1) feature reduction to find FC features based on functional edges that are associated with specific cognitive outcomes, (2) training of a predictive model using these features to predict cognitive outcomes, and (3) evaluation of the accuracy and generalizability of resulting models. Recent methodologies have been suggested for designing, interpreting, and assessing the performance of these models in an unbiased manner [17]. However, methodologies to assess how heterogeneity and reliability of FC training data affects predictive models and further methodologies to improve the quality of both FC fingerprinting and predictive models synergistically are still needed.

So far, work to improve the individual fingerprint of FC and predictive modeling of cognition from FC has run on parallel tracks, focusing on either the former or the latter aspect. Here, we unify the frameworks of differential identifiability [8] and connectome predictive modeling (CPM) [16] in order to assess the effect of increasing FC fingerprinting, using differential identifiability, on key properties of predictive models. Because differential identifiability requires at least two FC data sets per subject (i.e. test/retest), we show the utility of using test and retest FC sessions for validation of CPM, in addition to standard cross validation approaches (e.g., leave one out).

When choosing key properties to assess the quality of CPM for the purposes of predicting and understanding cognitive associations to the brain, it is important to keep in mind that interpretation of anatomical locations of the cognitive correlates of FC are as relevant as the accuracy of prediction [17]. Hence, confirming robustness in the identification of functional edges should precede model fitting and assessments of model accuracy. Further, it is important to note that the robustness of both edge selection and coefficient estimation can significantly influence model accuracy and generalizability. Therefore, we propose to evaluate three critical properties for *well-behaved* FC-based predictive models: (1) stability of edge selection and subsequent coefficient estimation, (2) specificity of edge selection, and (3) generalizability of the prediction. To evaluate how volatile CPM is to the heterogeneity and reliability of FC training data used, we evaluate these properties in a leave one out paradigm and in test versus retest sessions from the same subjects.

## 1.2 Opportunities in Alzheimer's Disease

The gradual progression of neurocognitive deficits in AD is particularly amenable to study the specificity of models that use individual level FC to predict cognition. Briefly, mild cognitive impairment (MCI) typically begins with episodic memory decline, is later accompanied by subtle deficits in other domains, and ultimately results in progressive functional impairment as the subject transitions through the mild, moderate and severe stages of dementia [19-22]. Within the AD spectrum there is much individual heterogeneity in terms of disease presentation and progression over time [22], making predictive modeling at the individual level important.

The association between FC changes and cognitive deficits in AD has been subject of intense study to date [13, 23, 24]. Changes in functional networks, primarily the default mode and frontoparietal networks, have been consistently replicated between diagnostic groups [25-27]. Recent studies indicate that FC data can predict individual level diagnostic status [28] and global cognitive decline [29] with reasonable accuracy. Several studies also show relationships between FC data and deficits in specific cognitive domains associated with AD [13, 23, 30]. In this work, beyond assessing group level associations to specific cognitive domains, we present a framework that improves the ability of FC to predict individual level deficits across cognitive domains and identify functional networks predictive of specific cognitive deficits in AD.

## 2 Methods

### 2.1 Subject Demographics and Cognitive Performance

Resting state fMRI and neurocognitive testing data from the second phase of the Alzheimer's Disease Neuroimaging Initiative (ADNI2/GO) were used. Our analyses included 82 participants from the original 200 ADNI2/GO individuals with resting state fMRI scans. Subjects were excluded if (1) their amyloid status was not available, (2) were cognitively impaired, but showed no evidence of amyloid-beta ( $A\beta$ ) deposition, and/or had (3) over 30% of fMRI time points censored due to artifacts or head motion, see Section 2.2 for details.  $A\beta$  status was determined using either mean PET Florbetapir standard uptake value ratio cutoff (Florbetapir > 1.1; UC Berkeley) or CSF  $A\beta$  level  $\leq 192$  pg/mls [5]. The rationale for excluding  $A\beta$ - cognitively impaired participants was to avoid confounding by non-AD neurodegenerative pathologies. Subjects were stratified into five categories based on their diagnosis and  $A\beta$  status: (1)  $A\beta$ - cognitively normal individuals ( $CN_{A\beta-}$ ,  $n = 15$ ), (2)  $A\beta+$  CN or pre-clinical AD ( $CN_{A\beta+}$ ,  $n = 12$ ), (3) early mild cognitive impairment due to AD ( $EMCI_{A\beta+}$ ,  $n = 22$ ), (4) late mild cognitive impairment due to AD ( $LMCI_{A\beta+}$ ,  $n = 12$ ), and (5) AD dementia ( $AD_{A\beta+}$ ,  $n = 21$ ).

We selected a total of six measures from the ADNI2/GO neurocognitive battery, ([www.adni-info.org](http://www.adni-info.org) for protocols) that exhibited a significant diagnostic group effect (Table 1, ANOVA  $p < 0.05$ ): AVLT immediate and delayed recall, clock drawing, Trails B, and Animal Fluency. The Montreal cognitive assessment (MOCA) was chosen as a representative clinical measure of global cognition. See Table 1 for details.

**Table 1.** Demographics and Neurocognitive Comparisons of Diagnostic Groups.

Variable Mean (SD)	CN <sub>Aβ-</sub> (n = 15)	CN <sub>Aβ+</sub> (n = 12)	EMCI <sub>Aβ+</sub> (n = 22)	LMCI <sub>Aβ+</sub> (n = 12)	AD <sub>Aβ+</sub> (n = 21)
Age (Years)	74.2 (8.8)	75.9 (7.0)	72.6 (5.2)	73.3 (6.1)	73.5 (7.6)
Sex (% F)	64.2	41.7	50	61.6	42.9
Years of Education	16.7 (2.3)	15.8 (2.6)	15.2 (2.6)	16 (1.8)	15.4 (2.6)
MOCA *	26.2 (2.6)	25.3 (2.9)	22.3 (4.5)	20.6 (7.1)	13.4 (5.2)
Auditory Verbal Learning Immediate Recall *	11.1 (3.0)	11.33 (2.9)	9.9 (3.0)	7.6 (2.4)	4.3 (1.6)
Auditory Verbal Learning Delayed Recall *	6.2 (4.3)	7.8 (3.8)	4.3 (4.0)	2.8 (2.8)	0.4 (0.9)
Boston Naming*	28.2 (2.0)	28.7 (1.1)	27.1 (3.1)	25.9 (5.0)	22.4 (6.4)
Animal Fluency *	21.1 (3.64)	20.1 (3.6)	18.8 (4.2)	17.4 (4.8)	12.3 (5.0)
Clock Drawing *	4.8 (0.4)	4.5 (1.0)	4.6 (0.5)	3.8 (1.3)	3.1 (1.3)
Trail Making B *	69.0 (22.6)	81.4 (19.6)	99.9 (43.1)	131 (89.0)	216.9 (75.6)

\* Significant group effect (Chi-squared or ANOVA as appropriate,  $\alpha = 0.05$ ). Values in parenthesis denote standard deviation

## 2.2 fMRI Data Processing

We used T1-weighted MPRAGE scans and EPI fMRI scans from the initial visit in ADNI2/GO (Philips Platforms, TR/TE = 3000/30ms, 140 volumes, 3.3 mm thickness, see [www.adni-info.org](http://www.adni-info.org) for detailed protocols) for estimation of FC matrices. fMRI scans were processed with an in-house MATLAB and FSL based pipeline as described in detail in Amico et al. [31]. This pipeline mainly follows guidelines by Power et al. [32, 33]. For purposes of evaluating reproducibility, we split the processed fMRI time series into halves (mimicking test and retest) and assigned each half for each subject as “RestA” or “RestB” randomly to avoid biases related to first versus second half of the scan. It is noteworthy that splitting an fMRI session mimics the most ideal test-retest scenario where all conditions are maintained.

We obtained two FC matrices from the RestA and RestB halves of the fMRI time-series for each subject. FC nodes were defined using a 278 region cortical parcellation [34], as detailed in Amico et al. [31], with modified subcortical parcellation [35], for a total of 286 gray matter regions. We estimated single session functional connectivity matrices by calculating the Pearson correlation coefficient ( $r_{ij}$ ) between the fMRI time-series of each pair of brain regions. Each region’s time-series was obtained by averaging time-series of all voxels assigned to that brain region. Regions were assigned to one of the seven cortical resting state subnetworks (RSN/RSNs): visual (VIS), somato-motor (SM), dorsal attention (DA), ventral attention (VA), limbic (L), fronto-parietal (FP), and default mode network (DMN) [36], with the remaining regions assigned to a subcortical (SUB) or cerebellar (CER) networks.

## 2.3 Differential Identifiability

Using group level PCA, we found the optimal FC reconstruction point to maximize RestA and RestB FC test-retest reproducibility, measured using differential identifiability ( $I_{diff}$ , Fig.1) [8]. The “identifiability matrix”

$I$  was defined as the matrix of pairwise correlations (square, non-symmetric) between the subjects'  $FC_{RestA}$  and  $FC_{RestB}$ . The dimension of  $I$  is  $N^2$  where  $N$  is the number of subjects in the cohort. Self-identifiability, ( $I_{self}$ , Eq. 1), was defined as the average of the main diagonal elements of  $I$ , consisting of correlations between  $FC_{RestA}$  and  $FC_{RestB}$  from the same subjects.  $I_{others}$  (Eq. 2), was defined as average of the off-diagonal elements of matrix  $I$ , consisting of correlations between  $FC_{RestA}$  and  $FC_{RestB}$  of different subjects. Differential identifiability ( $I_{diff}$ , Eq. 3) was defined as the difference between  $I_{self}$  and  $I_{others}$ .

$$I_{self} = \frac{1}{N} \sum_{i=1}^N I_{i,i} \quad (Eq. 1)$$

$$I_{others} = \frac{1}{2 \binom{N}{2}} \sum_{i \neq j} I_{i,j} \quad (Eq. 2)$$

$$I_{diff} = 100 * I_{self} - I_{others} \quad (Eq. 3)$$

We applied group level PCA [10] in the FC domain, on a data matrix (Fig. 1A-B) containing vectorized  $FC_{RestA}$  and  $FC_{RestB}$  (upper triangular of FC matrices excluding main diagonal) from all subjects. Following decomposition (Fig. 1C), we iteratively reconstructed (Fig. 1D) all FCs and quantified  $I_{diff}$  for a range of number of PCs (Fig. 1E). The reproducibility at the functional edgewise level for each subject was evaluated for the original FC matrices. FC matrices were reconstructed using the number of PCs optimizing  $I_{diff}$ . In order to minimize effects of outliers, we repeated the sampling 30 times selecting 50 of 82 subjects each time. The average edgewise ICC is reported.

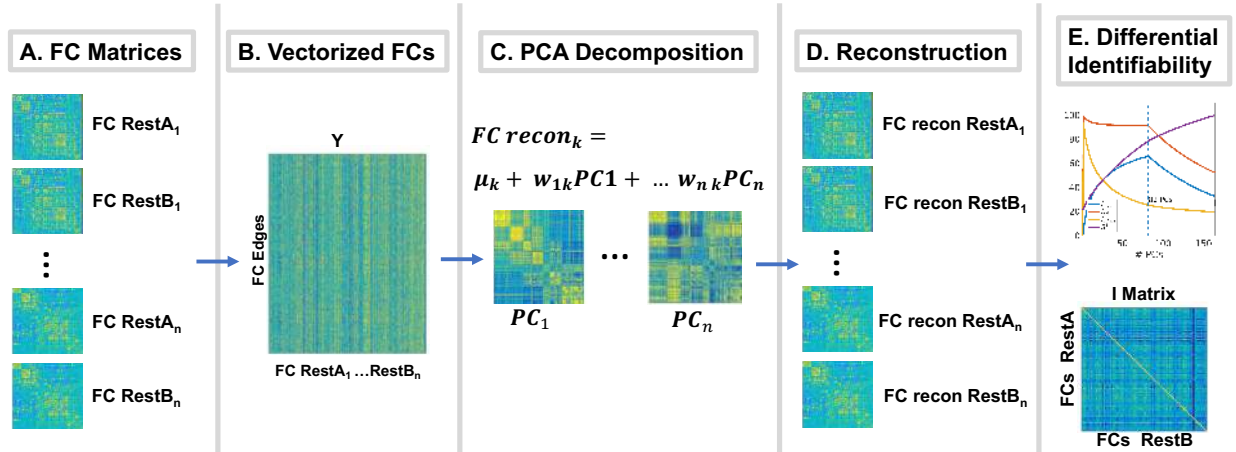


**Figure 1.** PCA decomposition and Differential Identifiability ( $I_{diff}$ ) scheme. **(A)** For each subject, two FC matrices (RestA and RestB) were estimated for each half of the fMRI time-series. **(B)** FC matrices were vectorized (upper triangular) and placed into a group FC matrix. **(C)** PCA decomposition was performed on the group FC matrix. Each PC can be arranged as a matrix in the FC domain. **(D)** Individual FCs were reconstructed using different number of PCs. **(E)**  $I_{diff}$  was estimated for different number of PCs (in order of explained variance) and the number of PCs maximizing  $I_{diff}$  found.

## 2.4 Connectome Predictive Modeling

We used the CPM [16] framework (Fig. 2) to model the prediction of outcome measures (section 2.1) from FC (Fig. 2A). Outcome measures were z-scored prior to CPM to allow for direct comparison between models across outcome measures. CPM consisted of three steps. First, we performed an *edge selection* process to identify significantly associated edges for a given outcome measure (Fig. 2B). This step resulted in a square, symmetric binary mask (286 x 286 regions) where edges significantly associated with a given outcome measure have a value of 1. We then fit a *linear model* to predict the outcome measure from FC within selected edges by adding their connectivity values per subject (Fig. 2C). Finally, we *validated* the

model using  $k$ -fold cross validation, where  $k$  depends on the data sample size (Fig. 2D). Here, we used a leave one out cross validation producing 82 instances of each predictive model.

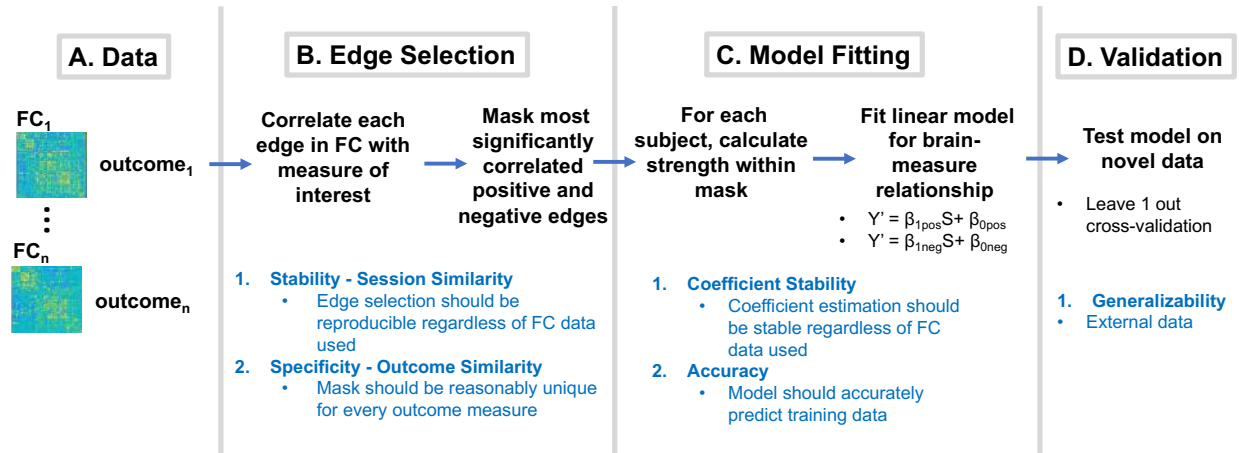


**Figure 2.** Connectome Predictive modeling scheme. Black text delineates procedures for each step while blue text delineates properties that are important to achieve an overall robust model. **(A)** Edgewise correlation of FC data with the outcome measure was performed. **(B)** A subset of significant edges (see 2.5.1) was used to create masks of positive and negative associations for each outcome measure. Stability of edge selection (regardless of FC training data) is important in this step. **(C)** A linear model was fit to assess associations between FC strength within the FC mask and the outcome measure. Coefficient stability for a given set of masks (regardless of FC training data) is important in this step. **(D)** Model generalizability to external data was assessed using a leave one out cross validation. It is important that the final model is generalizable to external data.

## 2.5 Unified Differential Identifiability – Connectome Predictive Modeling Pipeline

Our goal was to assess the effect of improving FC identifiability [8, 15] on CPM [16] of cognitive deficits in AD. We first used differential identifiability [5] to quantify how reconstructing individual FC data using group level principal component analysis (PCA) improved test-retest identifiability (Fig. 3A). We then evaluated how reconstructing FC at different numbers of PCs affected the performance of CPM (Fig. 3B-D). To assess the volatility of CPM across training datasets, we compared performance across leave one out iterations generated from the same FC session (“within session”, blue arrows). Additionally, we assessed how test-retest reliability in FC affected CPM by comparing performance between corresponding leave one out instances from different FC sessions of the same subjects (“between session”, green arrows). We evaluated stability of edge selection and coefficient estimation across leave one out instances “within session” (Fig.3 B-C green arrows) and “between session” (Fig. 3B-C blue arrows). We also evaluated specificity in edge selection across outcome measures. Finally, we evaluated the accuracy of models fit on RestA FC data in predicting cognitive outcomes from RestA FC data (Figs 1D green arrow) and how well those models generalized to predict cognitive outcomes from RestB FCs (Fig. 3D, blue arrow) using a leave one out paradigm.

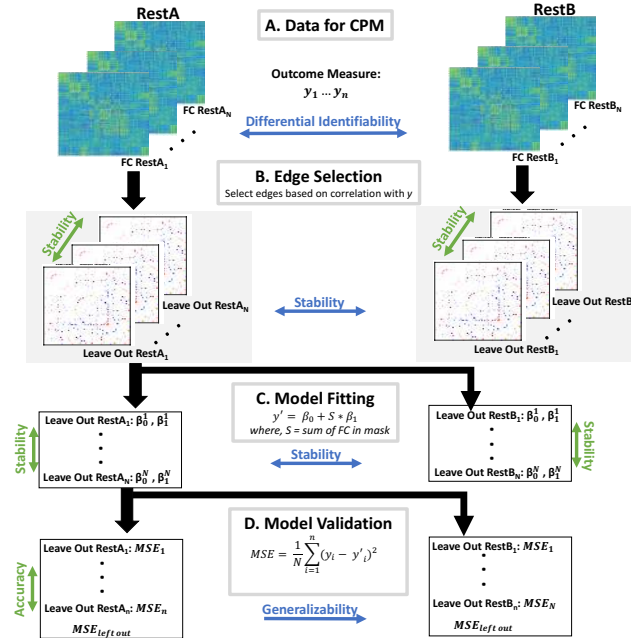


**Figure 3.** Unified Differential Identifiability – Connectome Predictive modeling pipeline. **(A)** Processed fMRI time series were split in half, generating two functional connectomes per subject per session (FC RestA, FC RestB). These FCs were decomposed and reconstructed using incremental PC ranges, in descending order of explained variance. Differential Identifiability was assessed for each FC reconstruction. Connectomes for each subject were paired with an outcome measure  $y$ . Subsequent modeling steps were performed iteratively with FCs reconstructed at all PC ranges. Assessments of performance at each step were done both “within session” (green arrows) and “between session” (blue arrows) **(B)** Edgewise correlation of FC data with the outcome measure was performed. Edges meeting defined significance criterion were selected, creating a mask for each outcome measure. Stability in edge selection between was evaluated. **(C)** A linear model was fit, modeling the association between FC strength within the RestA mask and the outcome measure. Coefficient stability between was assessed. **(D)** Model accuracy was assessed for RestA models, using a leave one out paradigm. Mask and coefficients from RestA were applied to RestB data, also in a leave one out paradigm, to evaluate the generalizability of the model.

### 2.5.1 Edge Selection and Mask Stability

Using measures of similarity, we evaluated (1) stability of edge selection for each outcome measure when the FC training data was varied both “within session” (Fig. 3B green arrows) and “between session” (Fig. 3B blue arrows) (*session similarity*) and (2) specificity in edge selection across measures for fixed FC training data (*outcome similarity*). As originally proposed in CPM [16], we estimated edgewise correlations and created masks for each leave one out instance of a given predictive model by selecting the edges in the top and bottom percentile for correlation with each outcome measure (404 edges per mask). We choose a percentile based edge selection such that masks for all outcomes measure contained the same number of edges, removing the effect of mask density when comparing *session similarity* and *outcome similarity*.

Similarity measures were assessed both on correlation matrices and masks associated with each outcome measure. We evaluated similarity in correlation matrices associated with each outcome using the Frobenius norm, where values close to zero denote high similarity between correlation matrices. We evaluated the similarity of the masks resulting from these correlation matrices using edgewise mask overlap jointly for positive and negative masks, where overlap values close to 1 denote high similarity between masks. Overlapping functional edges were required to exhibit a significant correlation of the same sign in both masks for outcome measures positively correlated to each other. To achieve high stability and specificity, the edge selection must show higher *session similarity* than *outcome similarity* implying that the outcome measure has a greater impact on edge selection than the session of FC data being used.

We first performed the assessment of stability described above on original FCs (reconstruction with all PCs) to evaluate variable edge selection in the original implementation of CPM on our data, which is representative of clinical quality resting-state fMRI data in neurodegeneration. We evaluated *within session similarity* by quantifying pairwise mask overlap of leave one out instances within RestA and within RestB. Note that in the “within session” leave one out scenario, every pair of masks were generated using the same 80 of the 81 FCs. We evaluated *between session similarity* by quantifying pairwise mask overlap between RestA versus RestB FCs. Note these data are from the same subjects but different “sessions” (as data were split into halves). Mean and full range were reported to evaluate overlap across all possible comparisons between masks.

Because of the variability observed in *session similarity* across leave one out masks (Table 2), we proceeded to create a consensus mask for all instances of the predictive model (i.e., one mask for each outcome measure). We applied bootstrapped random sampling [37] of the whole cohort (1,000 samples) to generate distributions of edge-wise Pearson correlations between each outcome and RestA FCs from each subject, using the bootstrap mean at each edge as the representative estimate. Masks were created using the percentile based approach mentioned above. This process was repeated using the remaining FC data (RestB). We then assessed *within session similarity* (RestA vs. RestB) and average pairwise *outcome similarity* across all PC ranges.

### 2.5.2 Model Fitting and Coefficient Stability

Using the edge selection from RestA FCs, we calculated FC strength within each mask for all FCs (i.e. the sum of the connectivity values for all the functional edges in the mask) and estimated two sets of coefficients for RestA and RestB FCs separately, using a leave one out paradigm. We applied a linear model (Fig. 3C) to fit the relationship between FC strength and each outcome measure separately for positive (positive model) and negative masks (negative model).

Analogous to the assessment of stability in edge selection, we evaluated stability of model fitting by assessing the effect of varying FC training data on coefficient similarity, using both “within session” and “between session” approaches. To evaluate “within session” similarity (Fig. 3C green arrows), we determined the standard deviation (SD) for each coefficient ( $\beta_0$  intercept,  $\beta_1$  slope) across leave one out iterations separately for RestA and RestB, thereby assessing similarity in coefficient estimation across FCs included in edge selection (RestA) versus across FCs not included in edge selection (RestB). To assess “between session” similarity (Fig. 3C blue arrows), we calculated the sum of squared errors (SSE) between RestA and RestB coefficients to assess the deviation between RestA and RestB coefficients derived from the “different sessions” of the FCs in the same subjects, where one of the sessions was used for edge selection and the other was not.

### 2.5.3 Model Accuracy and Generalizability

To assess model accuracy and generalizability, we designed a validation scheme (Table 2) that allowed us to separately assess the contribution to accuracy and generalizability when including an FC in edge selection versus coefficient estimation. We used RestA FCs (edge selection and coefficients) for model development, and RestB FCs as validation data. We first calculated mean squared error (MSE) on the RestA FCs used to fit each leave one out instance of the model (Training) and on RestA FCs left out (Testing). Note that all RestA FCs were used in edge selection. Model generalizability was then tested by imposing each leave one out model derived from RestA on RestB data. MSE was assessed for RestB FCs from subjects used to fit each model instance (Validation1) and on the left out subject (Validation2). Note that no RestB FCs were used in edge selection or model fitting.

**Table 2.** Scheme for evaluating model accuracy and generalizability.

	Model Development		Model Validation	
	Training	Testing	Validation1	Validation2
<b>FC Session</b>	RestA	RestA	RestB	RestB
<b>FC included in edge selection</b>	Yes	Yes	No	No
<b>Subject included in edge selection</b>	Yes	Yes	Yes	Yes
<b>FC included in coefficient estimation</b>	Yes	No	No	No
<b>Subject Included in coefficient estimation</b>	Yes	No	Yes	No

### 2.5.4 Alzheimer’s Disease Related Assessments

We used binomial tests ( $\alpha = 0.01$ ) for each outcome measure to assess whether specific RSNs (e.g. DMN-DMN), or their interactions (e.g. DMN-FP), were over represented in edge selection beyond what could be expected from 404 edges chosen at random. Only edges from overrepresented networks (or interactions) were visualized using BrainNet viewer [38] and the BioImage Suite [16].

## 3 Results

### 3.1 Differential Identifiability

Test-retest reliability (Fig. 4), as measured using  $I_{diff}$  peaked at 82 PCs (Fig. 4A,  $I_{diff} = 65.9$ ,  $I_{self} = 91.28$ ,  $I_{others} = 25.4$ ) which is equal to the number of subjects and explains 78.6% of the variance in the group FC data (Fig. 4A). We observed an almost two-fold increase in differential identifiability from 32.7 in raw data (with full 164 PCs) to 65 in the optimally reconstructed data (Fig. 2A). Such increase in whole level test-retest reliability was also observed when looking at individual functional edges where mean edge ICC (Fig.4B) increased from 0.40 (#PCs = 164) to 0.87 (#PCs = 82) (Fig. 4B).

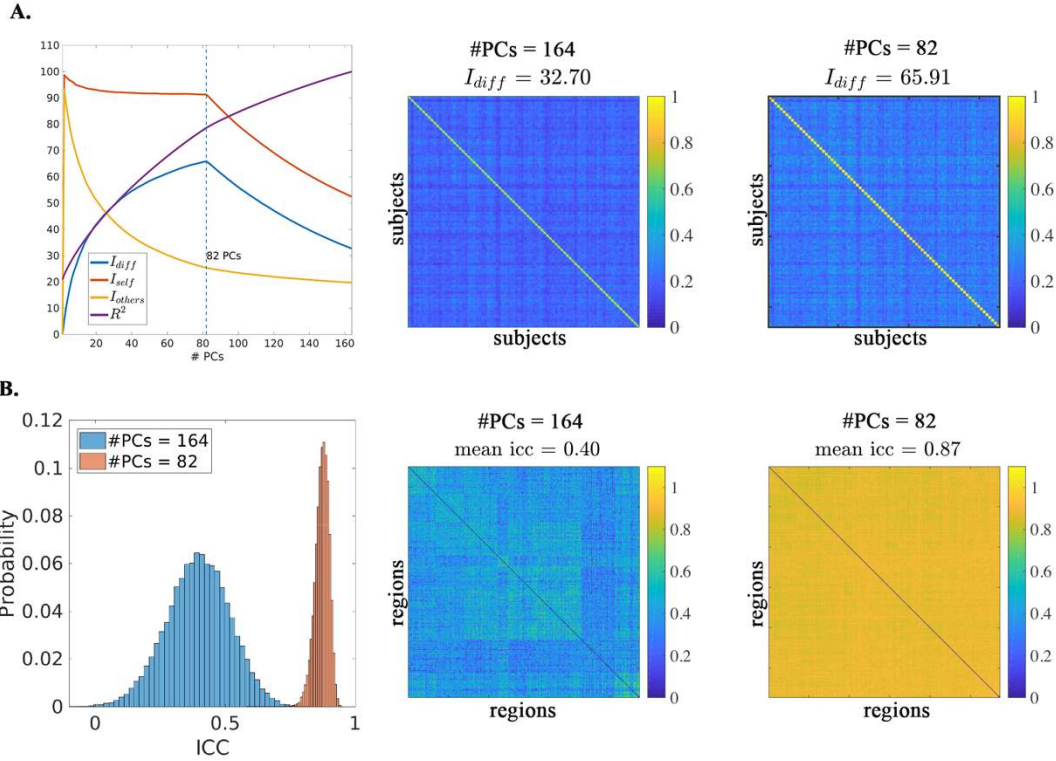


**Figure 4.** Identifiability assessment at the connectome level and edgewise. **(A)** Connectome level identifiability assessment.  $I_{self}$  and  $I_{others}$  represent similarity between test and retest FCs of the same vs different subjects, respectively, across number of PCs used for reconstruction. Differential identifiability ( $I_{diff}$ ) is the difference between  $I_{self}$  and  $I_{others}$ . The cumulative explained variance ( $R^2$ ) across number of PCs used for reconstruction is also included. **(B)** Edgewise level identifiability assessment showing edgewise ICC for original data and optimally reconstructed data. Identifiability and ICC matrices for optimally reconstructed and all (e.g., raw) data are also presented in **(A)** and **(B)**, respectively.

### 3.2 Connectome Predictive Modeling

#### 3.2.1 Edge Selection – Evaluation of Original CPM

Average mask similarity measured as mask overlap between leave one out instances of the same session (RestA or RestB) ranged from 73% (AVLT Delayed Recall) to 90% (MOCA) across outcome measures. Minimum mask overlap between leave out instances from the same session ranged from 20% (Boston Naming) to 75% (MOCA), while maximum overlap ranged from 96% (AVLT Immediate Recall) to almost 100% (MOCA, TrailsB). Mask overlap between leave one out instances of different sessions (RestA vs. RestB) was significantly lower than leave one out instances from the same sessions. Remarkably, there was no significant difference in overlap when corresponding leave one out instances were compared versus when non-corresponding leave one out instances were compared (around 3% Clock Score to around 47% MOCA in both cases).

**Table 3.** Leave One Out Mask Overlap in original CPM.

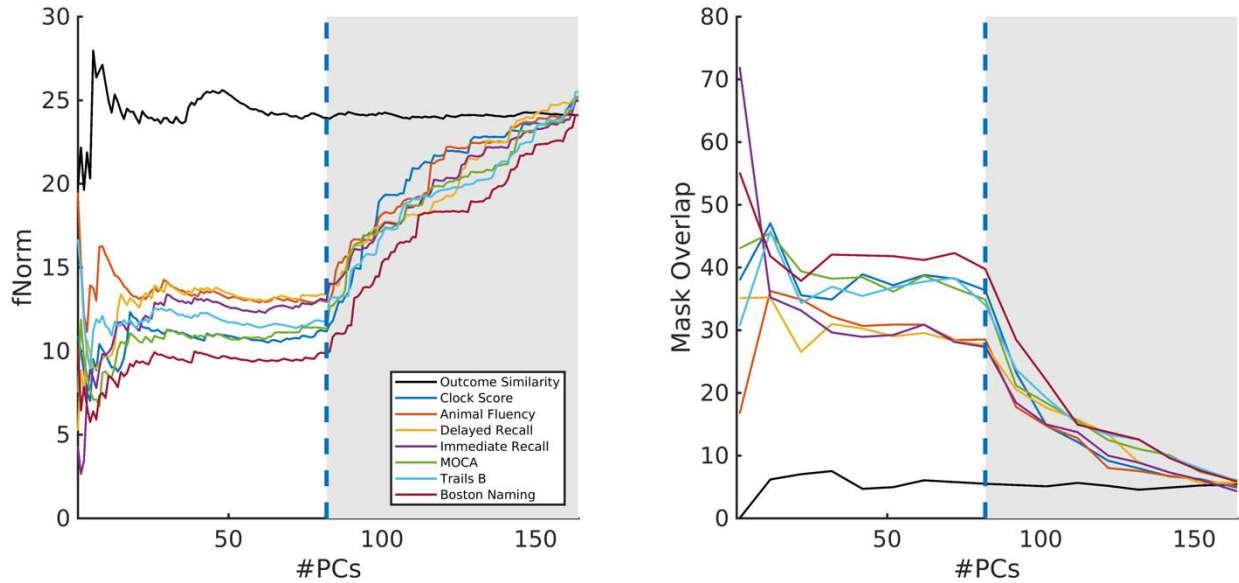
Outcome Measure	Session Similarity – Original CPM		
	Mean [Min Max]	Percent Overlap	
	Within Session	Between session Same Subjects	Between Session Different Subjects
MOCA*	89.7 [74.6 99.8]	47.3 [46.6 47.9]	47.1 [46.1 47.6]
Auditory Learning Immediate Recall *	72.0 [49.1 95.5]	3.6 [2.7 4.3]	3.6 [2.3 4.6]
Auditory Learning Delayed Recall *	72.8 [36.2 95.6]	3.2 [2.4 4.1]	3.2 [1.9 4.2]
Boston Naming *	76.5 [19.6 96.9]	4.3 [3.16 5.66]	4.17 [2.1 5.6]
Animal Fluency *	74.4 [40.9 97.5]	5.5 [4.3 6.4]	5.4 [3.6 6.4]
Clock Drawing*	73.7 [34.8 95.9]	2.45 [2.0 3.1]	2.4 [1.8 3.5]
Trail Making B *	89.4 [71.5 99.8]	44.0 [43.5 44.8]	43.9 [41.1 44.6]

\*Indicates significant difference in leave one out mask overlap “within session” versus “between session” (95% CI)

### 3.2.2 Edge Selection – Stability and Specificity

Stability in edge selection, quantified by *session similarity* between RestA and RestB edge selection, exhibited an optimal and stable range between 35-82 PCs both in terms of correlation matrices and resulting masks associated to each outcome. *Session similarity* in correlation matrices associated to each outcome measure (Fig.5A) exhibited stable range of minimal divergence between RestA and RestB (35 to 82 PCs) after which divergence began to monotonically increase for all outcome measures. *Session similarity* in masks, as measured by overlap (Fig.5B) between RestA and RestB, exhibited an optimal range of overlap (29% AVLT Immediate Recall – 43% Boston Naming) in the range of 35-82 PCs, then monotonically decreased after 82 PCs for all outcome measures.

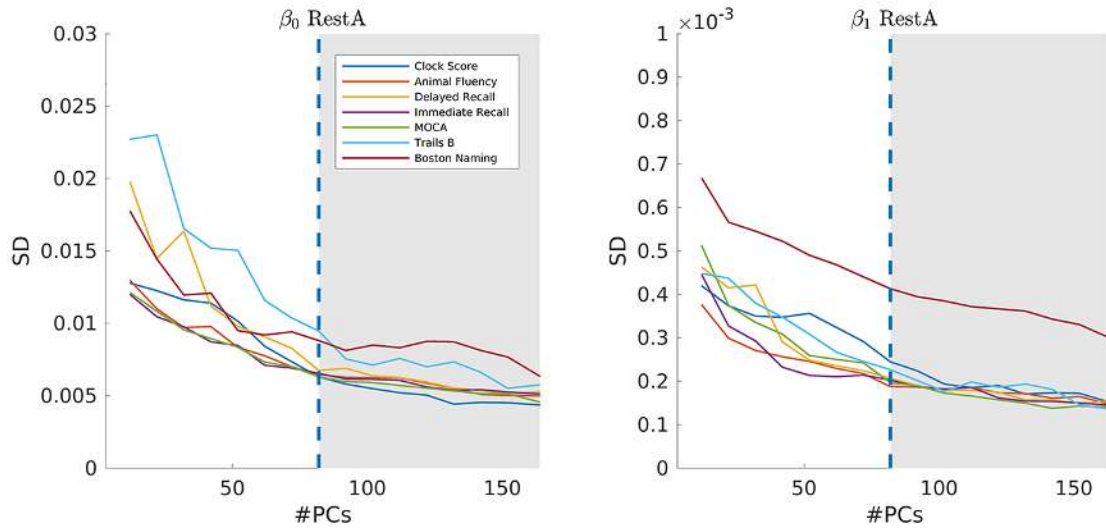
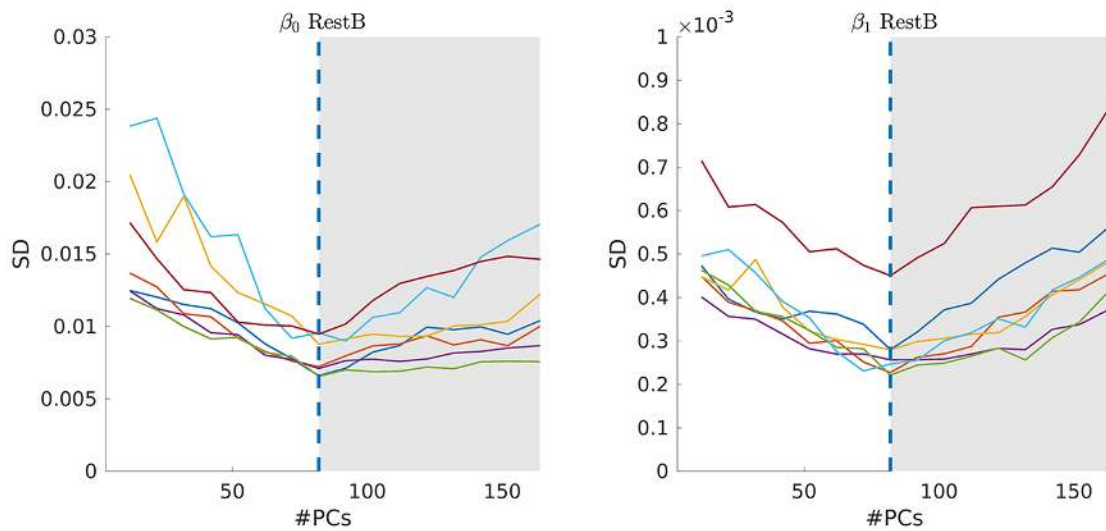
Outcome similarity, quantified by average, pairwise *outcome similarity* in edge selection for RestA FCs, remained relatively stable across the entire PC range, both in terms of correlation matrices (Fig.5A black line) and resulting masks (Fig.5B black line). After 82 PCs, *session similarity*, both in terms of Frobenius norm and mask overlap, began to approach *outcome similarity*, indicating that past 82 PCs edge selection begins to lose stability with regard to the training data used to perform edge selection.



**Figure 5.** (A) (Black line) Average pairwise Frobenius Norm of correlation matrices between outcome measures and RestA FCs. (Colored Lines) Frobenius norm of correlation matrices associated to each outcome measure for RestA FCs versus RestB FCs. (B) (Black Line) Average pairwise overlap between masks derived from RestA FCs for different outcome measures. (Colored Lines) Mask overlap between RestA FCs versus RestB FCs, for the same outcome measure.

### 3.2.3 Model Fitting - Coefficient Stability

The observed variability in coefficients estimated from leave one out iterations using RestA FCs was minimal and stable for a wide range of PC numbers, from 82-164 PCs (Fig. 6A-B, Fig.5A-B). In contrast, variability in coefficients estimated from leave one out iterations using RestB FCs was minimized at 82 PCs (Fig.6 C-D, Fig.7 C-D). Thus, for FCs not included in edge selection, coefficient variability was minimized at the exact point where  $I_{diff}$  was maximized. Additionally, divergence in coefficient estimation between RestA and RestB was stable for both coefficients until 82 PCs, then began to monotonically increase (Fig. 8). Thus, at the point of maximal  $I_{diff}$ , divergence in coefficient estimation between FCs included in edge selection (RestA) and FCs not included in edge selection (RestB) was still within the optimal range.

**A.****Negative Model****B.**

**Figure 6.** Standard deviation (SD) in negative model coefficients ( $\beta_0$  intercept,  $\beta_1$  slope) across leave one out instances. Note that RestA FCs were used in edge selection while RestB FCs were not. (A) Standard deviation in coefficients from RestA negative model. (B) Standard deviation in coefficients from RestB negative model.

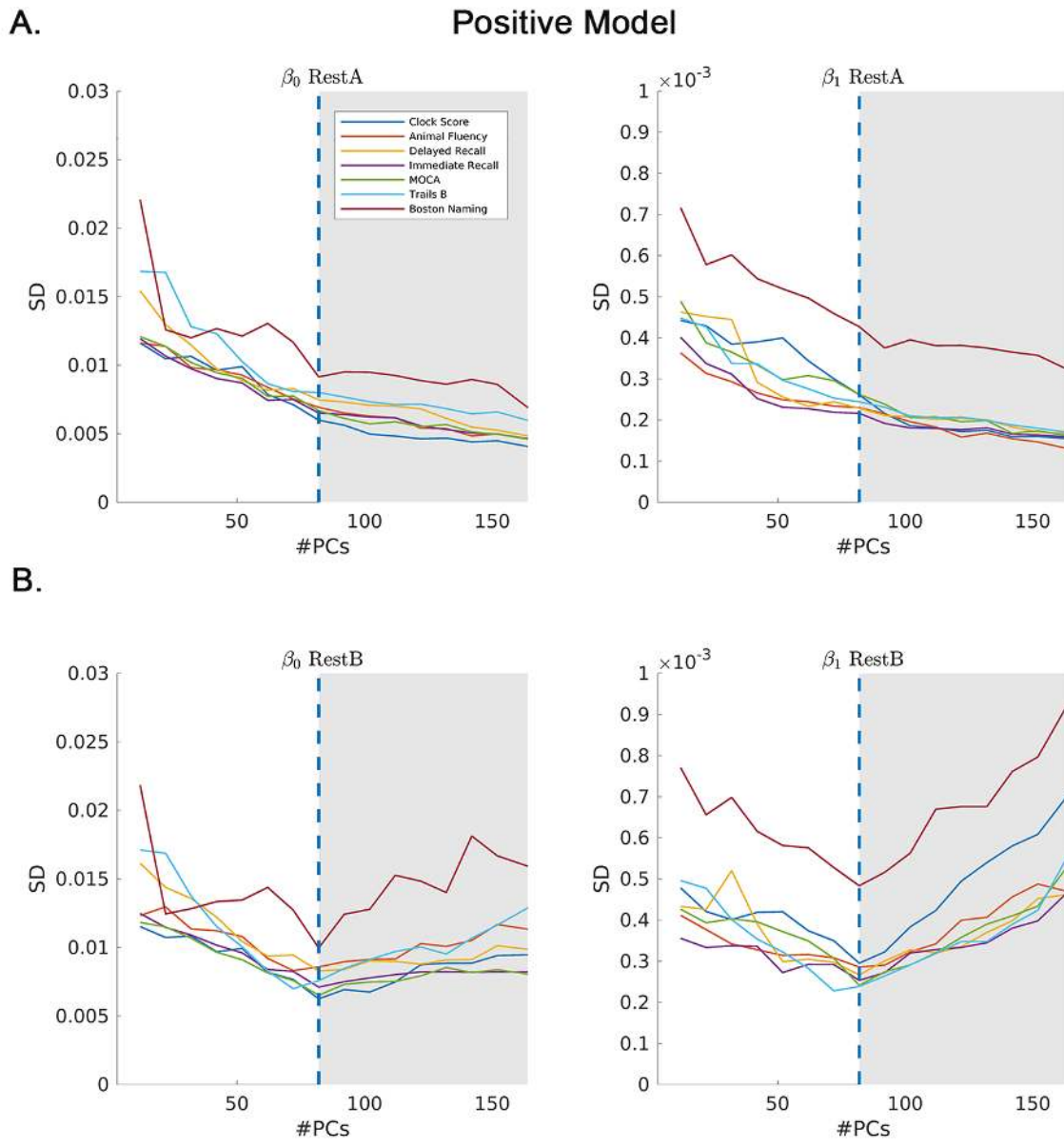


**Figure 7.** Standard deviation (SD) in positive model coefficients ( $\beta_0$  intercept,  $\beta_1$  slope) across leave one out instances. Note that RestA FCs were used in edge selection while RestB FCs were not. (A) Standard deviation in coefficients from RestA positive model. (B) Standard deviation in coefficients from RestB positive model.

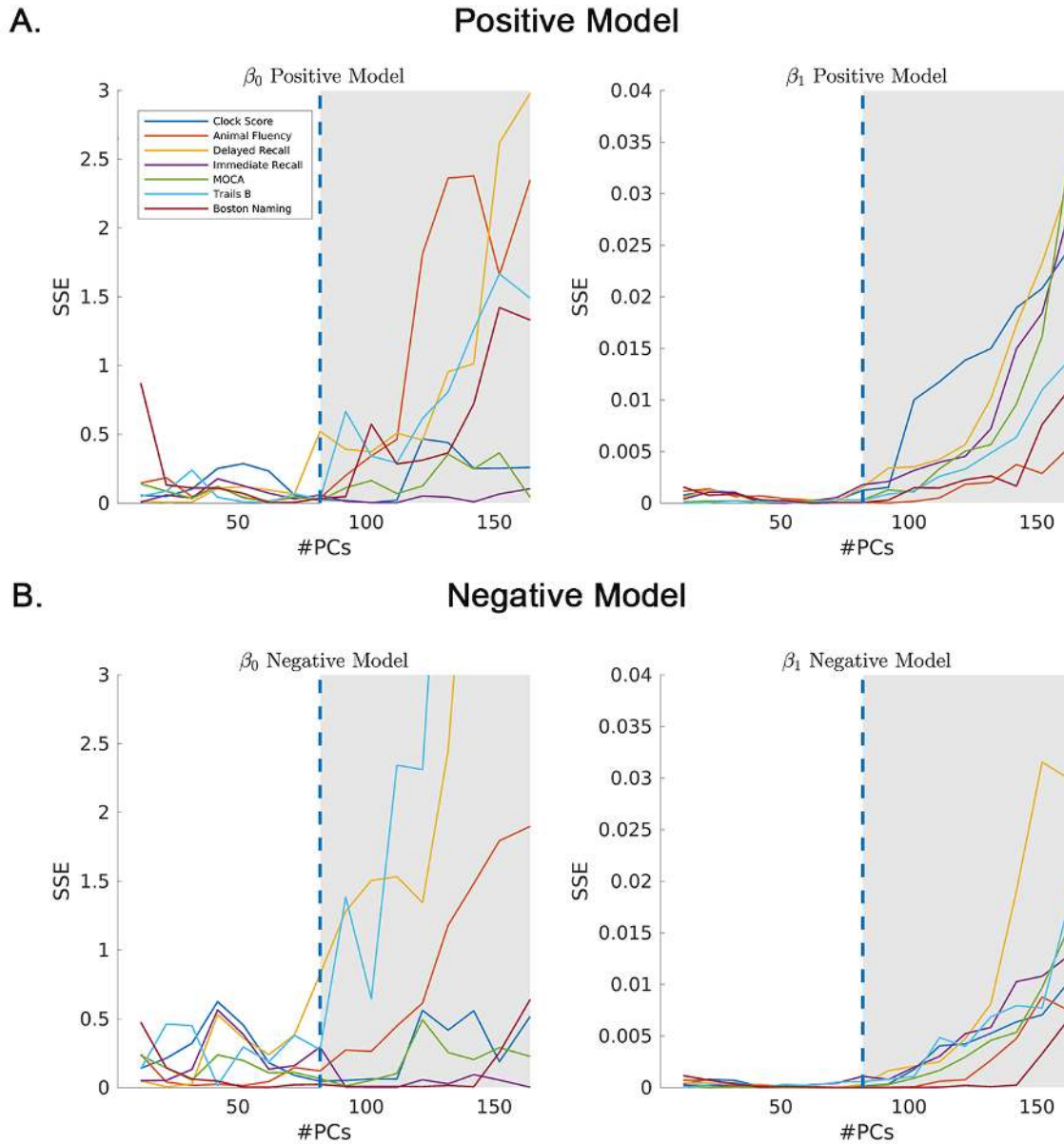


**Figure 8.** Divergence, measured as sum of squared errors (SSE), between leave one out coefficients ( $\beta_0$  intercept,  $\beta_1$  slope) estimated from RestA versus RestB. Note that RestA FCs were used in edge selection while RestB FCs were not included. **(A)** SSE between  $\beta_0$  coefficients for negative and positive models. **(B)** SSE between  $\beta_0$  coefficients for negative and positive models.

### 3.2.4 Model Accuracy and Generalizability

At the model development step, where MSE was evaluated on FCs used in edge selection (RestA), MSE was lowest for the full range of PCs (raw data, Fig.9A,C) in both Training and Testing subjects. In contrast, at the validation step when model accuracy was evaluated on FCs not participating in edge selection (RestB), MSE was minimized at the optimal FC reconstruction for  $l_{diff}$  (82 PCs) (Fig.8B&D), for both Validation1 subjects (RestA FCs included in model fitting) and Validation2 subjects (RestA FCs not included in model fitting), see Table2 for details. These relationships held true across outcome measures and for both positive (Fig.9A-B) and negative models (Fig.9C-D).

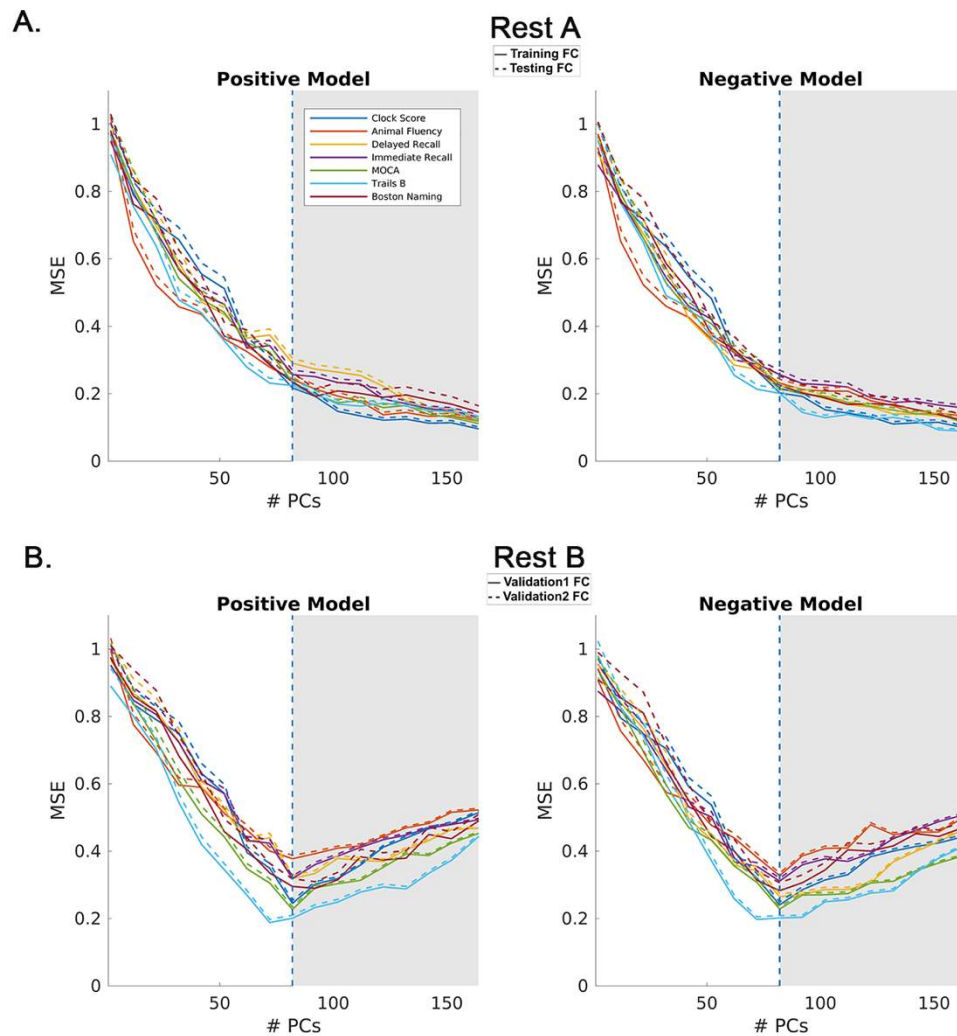


**Figure 9.** For all plots, RestA FCs were used for edge selection and model fitting. Using a leave one out approach for testing, 82 iterations of each model were fit. In-sample validation was performed by assessing the performance of the models on training (solid lines) versus testing subjects (dashed lines). **(A)** Model performance on RestA FCs. Here solid lines are FCs included in edge selection and in training of the model (Training FCs), while dashed lines are FCs only included in edge selection (Testing FCs). **(B)** Model performance on RestB FCs. RestB FCs were not included in edge selection or model development. However, solid lines (Validation1 FCs) delineate performance of the model on RestB FCs from subjects whose RestA FCs were included in edge selection and model development, while dashed lines delineate performance on RestB FCs from subjects whose RestA FCs were only included in edge selection (Validation2 FCs).

### 3.2.5 Alzheimer's Disease Related Assessments

As we assessed RSNs that were overrepresented in associations with various AD related cognitive deficits, several motifs emerged (Table 4, Fig.10, Fig.S1-S6). Within and between DMN and FP network connections were associated with all outcome measures (Fig.10, Fig.S1-S6). Decreased connectivity between ventral attention and frontoparietal networks was associated with poorer performance on outcomes with significant attention components (AVLT Immediate recall Fig. S2, Boston Naming Fig. S4, and TrailsB Fig. S6). Connectivity between dorsal attention (DA) and visual networks, stemming from a DA node in the parietal cortex, was negatively associated with performance on language measures (Animal

Fluency Fig. 10 and Boston naming Fig. S4). In contrast, limbic-default mode network connections were positively associated with performance on these cognitive outcomes. Additionally, within and between network connectivity of the visual network to somatomotor and both attentional networks was associated, positively and negatively, with performance on Animal Fluency (Fig. 10), a task known to evoke visual imagery. Increased intra-cerebellar connectivity was associated with poorer performance on TrailsB (Fig. S6), the only task with a heavy subconscious motor component.

**Table 4.** Significantly Overrepresented Resting State Networks for each outcome measure. RSNs (e.g. DMN-DMN) or their interactions (e.g. DMN-FP) represented above chance in edge selection (binomial test,  $\alpha = 0.01$ ). RSN abbreviations: visual (VIS), somato-motor (SM), dorsal attention (DA), ventral attention (VA), limbic (L), fronto-parietal (FP), and default mode network (DMN), subcortical (SUB), and cerebellar (CER) network.

<b>Significant Resting State Networks</b>		
<b>Outcome Measure</b>	<b>Positive Mask</b>	<b>Negative Mask</b>
<b>MOCA</b>	VIS-VA	VIS-DMN
	DA-VA	DA-CER
	L-FP	VA-FP
	L-CER	FP-FP
<b>Auditory Learning Immediate Recall</b>	VIS-SM	SM-SUB
	VIS-VA	VA-FP
	SUB-CER	VA-DMN FP-FP
<b>Auditory Learning Delayed Recall</b>	VIS-SM	VA-FP
	L-CER	FP-DMN
	FP-CER	DMN-DMN
<b>Boston Naming</b>	VIS-VIS	VIS-DA
	SM-FP	VIS-DMN
	L-DMN	SM-SUB
	FP-SUB	SM-CER
	DMN-SUB	VA-FP FP-FP
<b>Animal Fluency</b>	VIS-VIS	VIS-DA
	VIS-SM	VIS-DMN
	VIS-DA	SM-SUB
	VIS-VA	DA-DMN
	L-FP	VA-FP
	L-DMN DMN-DMN	
<b>Clock Drawing</b>	VIS-SM	VIS-DMN
	SM-FP	VIS-SUB
	FP-DMN	SM-SUB
	FP-SUB	DA-SUB
	SUB-SUB	
<b>Trail Making B</b>	VA-FP	SM-VA
	DMN-CER	DA-DA
		DA-FP
		L-CER CER-CER

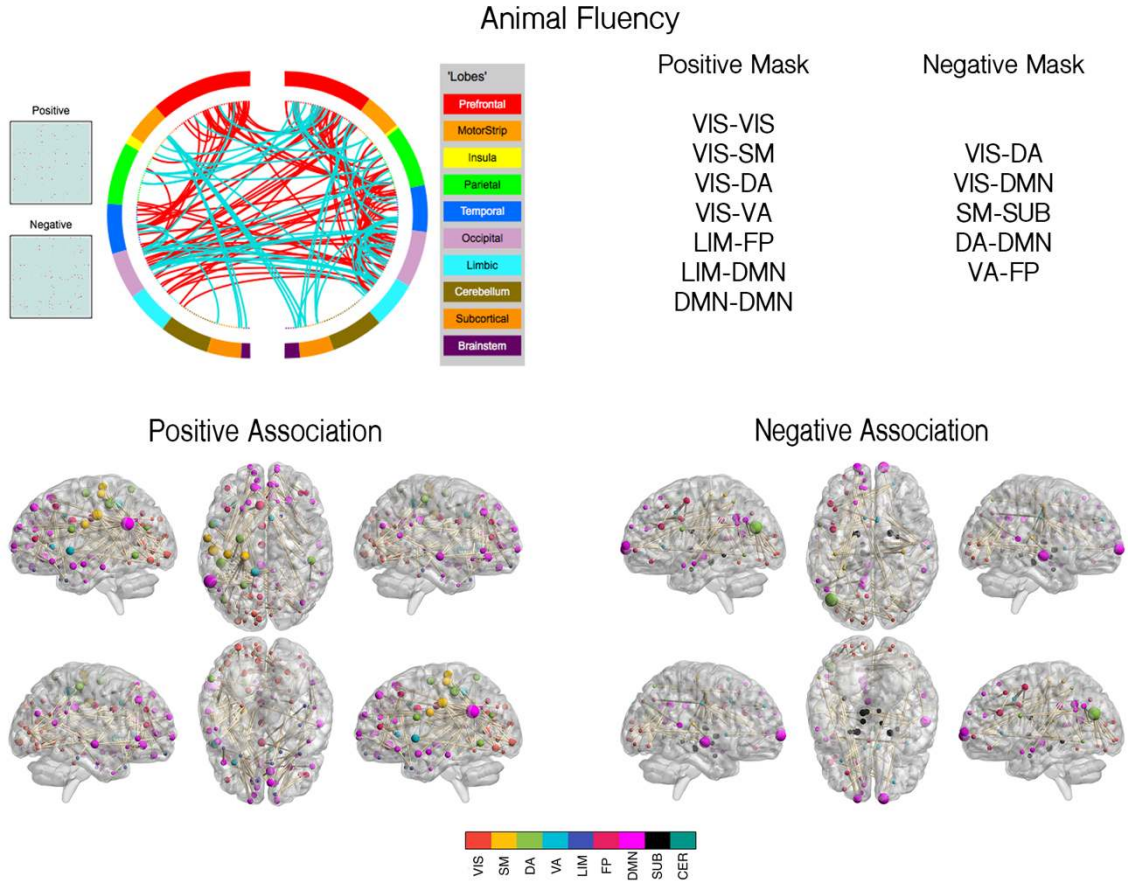


**Figure 10:** Over represented edges (binomial test,  $\alpha = 0.01$ ) for the Animal Fluency Test. (Top Left) Cluster gram delineating anatomical locations and sign of over represented edges (blue – positively associated edges, red – negatively associated edges). (Top Right) RSNs that are over represented beyond change. (Bottom) Glass brain plot of over represented edges where nodes are weighted by degree and colored according to RSN. Positively associated edges (left) and negatively associated edges (right) are visualized separately.

## 4 Discussion

Our work provides a comprehensive whole brain and whole cognitive spectrum view on the relationship between connectivity and cognition in AD and makes progress towards making individual level predictions of cognition from FC biomarkers. We accomplished that by improving the robustness of connectome predictive models of AD using differential identifiability, which allowed us to more confidently predict cognition from external FC data and identify FC motifs associated with cognitive deficits in AD.

### 4.1 Differential Identifiability

The implementation of FC as a biomarker in clinical use requires major advancements in individual level identifiability of FC. In this work, we improve individual level FC identifiability, as measured using differential identifiability, using group level PCA. As demonstrated by other datasets [5], the number of PCs necessary to optimize differential identifiability corresponded to the number of subjects in the cohort (Fig. 4A). This indicates that, while the dimensionality of the input data is twice the number of subjects (due to inclusion of test and retest data), the *subject dimensionality* of the data is the cutoff for a more accurate representation of individual functional connectomes. Also, as shown previously [8], optimizing  $I_{diff}$ , a coarse whole brain measure, also robustly increased edge wise test-retest reliability for most of functional edges (Fig. 4B). Optimal reconstruction retained 42% of the variance in the data, indicating that over half of the variance present in individual FC estimates is not representative of robust individual characteristics, despite the

extensive BOLD time series level cleaning (see Methods). Additionally, we note that  $I_{diff}$  for this dataset is much higher than what we saw in previous data where  $I_{diff}$  was optimized by splitting the resting state time series in half [8], highlighting that datasets with coarse temporal acquisition or datasets including clinical populations may benefit greatly from this group level PCA cleaning technique in order to improve individual level estimates of FC.

## 4.2 Edge Selection - Stability and Specificity

We first tackled the challenges in defining a set of FC connections that are associated with cognitive deficits in AD by using similarity measures to robustly assess edge selection using permutation of FC training data “within session” and “between session”. We found pairwise mask overlap for “within session” FCs to be high (average range: 72% - 90%) in spite of the observed high variability across pairs of leave one out instances (full range: 20% - 99%). It is noteworthy to remark that these masks were estimated through a leave one out procedure, hence all of them sharing 80 of 81 FCs. In contrast, overlap was poor for “between session” FCs, regardless of whether pairs of FCs from the same subjects versus FCs from different subjects were being compared. A poor overlap between masks reflects a very divergent edge selection, prohibiting generalizability in the identification of critical functional connections associated with the outcome measures.

Because one of the ultimate clinical goals of CPM is to identify critical neural networks associated with specific cognitive deficits, we proposed to create a consensus mask for each outcome measure based on bootstrapped random sampling. This additionally allowed for comparison of models estimated across leave one out instances, aiding in the ultimate goal of defining a single model for prediction of cognition from FC. A possible criticism of this procedure is that edge identification using the entire subject cohort precludes clear separation of training and testing data. To overcome this issue, we took advantage of previous splitting of fMRI data into RestA and RestB. Therefore, edge identification was done separately for RestA vs. RestB FCs, allowing for validation of RestA masks and models on RestB data.

Using differential identifiability as a criterion for FC reconstruction, we were able to improve the robustness of CPM in identifying neural networks associated to specific cognitive deficits. Overall, stability (*session similarity*) of edge selection displays an optimal regime (35-82 PCs), after which it exponentially decayed for all outcome measures (Fig. 6 colored lines). Overlap between RestA and RestB edge selection (Fig. 6B) for optimally reconstructed data (average overlap 35% across outcome measures) increased by an average of 25% from raw data (average overlap < 10% across measures). Reconstructing FC at different PC ranges did not affect the relative specificity in edge selection across outcome measures (*outcome similarity*, Fig. 6 black lines). However, past the optimal reconstruction point for differential identifiability, *session similarity* began to approach *outcome similarity*. Thus, past the optimal range, the FC session being used began to exhibit the same level of effect on edge selection as the outcome measure being used. This critically hampers the goal of finding underlying, robust brain networks associated with specific cognitive outcomes. In contrast, when FC was reconstructed at the optimal point for  $I_{diff}$ , the outcome measure matters more in edge selection than the applied FC session

### 4.2.1 Model Fitting - Coefficient Stability

Using differential identifiability as a criterion for FC reconstruction also improved stability of coefficient estimation in CPM. By using the edge selection from RestA to fit models on both RestA and RestB FCs, we assessed the effect of including versus excluding an FC in edge selection on coefficient estimation. For FCs included in edge selection (RestA FCs, Fig. 7-8A), reconstructing FC at the optimal point for differential identifiability did not have an effect on “within session” coefficient variability. The SD in coefficient estimation across leave one out instances decreased linearly until 82 PCs, then continued to decrease slightly until 164 PCs for both the positive and negative models. In contrast, when FCs were not included in edge selection (RestB FCs, Fig. 7-8B), coefficient variability was minimized at 82 PCs for both positive and negative models. Additionally, *between session* coefficient variability (SSE) was minimal and stable until 82 PCs, then began to increase monotonically until 164 PCs.

### 4.3 Model Accuracy and Generalizability

In addition to improving robustness of edge selection and parameter estimation in CPM, we also improved prediction of cognition from external FC data by using differential identifiability as the criterion for FC reconstruction. We assessed the influence of coefficient estimation versus edge selection on model accuracy and generalizability across PC ranges by comparing MSE in the model development versus model validation steps. We first assessed the influence of coefficient estimation in the model development step where all RestA FCs were included in edge selection, but one FC was left out of coefficient estimation for each instance of the model. We found that if an FC was included in edge selection, then whether that same FC was included in coefficient estimation or not (Fig. 9A, solid and dashed lines, respectively) the observed pattern of MSE changes over the range of numbers of PCs in any outcome measure remained the same. A steep drop in MSE was observed as 82 PCs were reached, then MSE modestly decreased over the rest of the PC range for both Training and Testing subjects. We then assessed the influence of edge selection in the Validation step by using the masks and models estimated from RestA FCs in estimation of outcome measures from RestB data, in a leave one out fashion. Here, none of the FC data was used in the edge selection or coefficient estimation steps. However, all of the RestA data of the same subjects was included in edge selection, while the RestA data from one subject was left out of coefficient estimation at each instance of the model. In contrast to coefficient estimation, whether an FC was included in edge selection (Fig. 9A, RestA FCs) or left out of edge selection (Fig. 9B RestB FCs) had a large influence on MSE changes over the range of PCs across all outcome measures. RestB FCs exhibited a clear minimization of MSE at 82PCs. This was equivalent for subjects whose RestA FC was included in coefficient estimation (Validation1) and for subjects whose RestA FC was left out of coefficient estimation (Validation2). Thus, masks and models fit on FC data reconstructed past the 82 PCs, appear to be over fitting to the idiosyncrasies in the RestA training data.

### 4.4 Alzheimer's Disease Related Assessments

We assessed whole brain connectivity in association to a representative spectrum of cognitive deficits in AD. We identified RSN components playing significant roles in prediction of each cognitive outcome and then assessed patterns in RSNs involved across cognitive outcomes. We identified RSN components or their interactions, that played significant roles in predicting cognitive outcomes as well as RSNs that played global roles in prediction of cognitive outcomes (Table 3). For instance, the dorsal attention and frontoparietal network connectivity was consistently associated with cognitive tasks that included a large attention component, consistent with a study showing that interaction between these networks plays a critical role in perceptual attention [39]. Impaired connectivity between these networks is also associated with cognitive decline in AD measured by increasing clinical dementia rating score [40]. We also identified that interactions between the visual network and other RSNs were consistently associated with tasks that required item generation in the context of verbal memory retrieval (i.e., AVLT, MOCA) or spontaneous generation of items belonging to a given category (i.e., Animal Fluency). This finding suggests an interactive role of the visual system with other parts of the brain when executing tasks requiring semantic organization and imagery. This role of the visual system is supported by other studies identifying activation of the visual cortex and cognitive networks in imagery and semantic association tasks [41, 42]. Additionally, the visual cortex has also been implicated in visual short term memory and working memory [41]. Furthermore, in AD, visual network connectivity has been previously associated to neurofibrillary tangle deposition [43] and with cognitive complaints in cognitively normal or MCI subjects [13]. Finally, we identified that frontoparietal and default mode network were associated with all cognitive outcomes. The central role of these networks in AD [26, 40, 44, 45] and their strong associations with amyloid [26, 46-48] and tau deposition [43, 47, 49] has been consistently documented.

### 4.5 Limitations and Future work

The unified identifiability-CPM framework proposed here provides many opportunities for improving the clinical utility of FC. An important and necessary step to improve the clinical utility of FC is to evaluate results obtained using this unified framework on an external dataset such as ADNI3, which includes similar acquisition and available cognitive outcomes. This will require the estimation of final hyper parameters from the ensemble of those estimated here, for instance by averaging coefficients obtained across leave one out

instances. In addition to external validation of the framework proposed here, our results indicate that there are other opportunities to improve both edge selection and predictive capability of FC. Despite showing significant improvement in robustness of edge selection using our framework, we were still under 40% “between session” overlap in edge selection for all outcome measures. This may indicate that further investigation into the impact of the scan length on edge selection should be assessed. Edge selection may also be improved by taking into account the network relationship between edges, as opposed to using edgewise correlation with thresholding which treats edges as independent entities. Additionally, assessments of within and between RSN edges and their associations with individual cognitive outcome measures indicate that these edges have distinct relationships with cognitive outcomes. CPM models may be improved by estimating separate coefficients for within and between RSN strength. Finally, CPM traditionally uses strength as the summary measure for the edges associated with each outcome. However, the edge selection step of CPM can be thought of the identification of a subgraph/network associated with that outcome. Therefore, summarizing edges using other graph theory metrics of both network integration and segregation may provide additional predictive power. Finally, CPM may also prove useful in predicting change in cognitive outcomes over time. Finally, assessing the utility of CPM to predict longitudinal outcomes in AD would be a worthy contribution towards improving FC utility as a clinical biomarker.

## **5 Conclusions**

Our framework improved the robustness of individual level prediction of cognition from FC, which is the first step towards clinical use of FC and better understanding of how functional connectivity supports cognition in AD. We showed that the joint framework of differential identifiability with connectome predictive modeling improves the quality of models obtained from CPM. Additionally, we showed that the use of two FC sessions from each subject provides a unique perspective when assessing and validating connectome predictive models. Collectively, our results indicate that robustness in the edge selection step is the most crucial aspect towards generalizability. Finally, in improving the robustness of CPM using differential identifiability, we performed a comprehensive assessment of the associations between functional connectivity and cognitive deficits in AD, across the whole brain and across the spectrum of deficits observed in AD. Our findings indicate both specific and global associations of resting state functional connectivity with cognitive deficits in AD.

**Funding:** This work was supported by the National Institutes of Health NIA F32AG062157, NIA R56, AG057195/U01 AG057195, NIA R01AG057739, NIA R01 AG040770, NIA K02 AG048240, NIA P30 AG010133, NIA U01 AG02490, NIH R01EB022574, NIH R01MH108467, the Baekgaard family, the Indiana Alcohol Research Center P60AA07611, and the Purdue Discovery Park Data Science Award "Fingerprints of the Human Brain: A Data Science Perspective".

## 6 References

1. Montague, P.R., et al., *Computational psychiatry*. Trends Cogn Sci, 2012. **16**(1): p. 72-80.
2. Bullmore, E. and O. Sporns, *Complex brain networks: graph theoretical analysis of structural and functional systems*. Nat Rev Neurosci, 2009. **10**(3): p. 186-98.
3. Fornito, A. and E.T. Bullmore, *Connectomics: a new paradigm for understanding brain disease*. Eur Neuropsychopharmacol, 2015. **25**(5): p. 733-48.
4. Yahata, N., K. Kasai, and M. Kawato, *Computational neuroscience approach to biomarkers and treatments for mental disorders*. Psychiatry Clin Neurosci, 2017. **71**(4): p. 215-237.
5. Yamada, T., et al., *Resting-State Functional Connectivity-Based Biomarkers and Functional MRI-Based Neurofeedback for Psychiatric Disorders: A Challenge for Developing Theranostic Biomarkers*. Int J Neuropsychopharmacol, 2017. **20**(10): p. 769-781.
6. Braun, U., et al., *Test-retest reliability of resting-state connectivity network characteristics using fMRI and graph theoretical measures*. Neuroimage, 2012. **59**(2): p. 1404-12.
7. Amico, E., A. Arenas, and J. Goni, *Centralized and distributed cognitive task processing in the human connectome*. Netw Neurosci, 2019. **3**(2): p. 455-474.
8. Amico, E. and J. Goni, *The quest for identifiability in human functional connectomes*. Sci Rep, 2018. **8**(1): p. 8254.
9. Svaldi, D., et al., *Towards Subject and Diagnostic Identifiability in the Alzheimer's Disease Spectrum Based on Functional Connectomes in Graphs in Biomedical Image Analysis and Integrating Medical Imaging and Non-Imaging Modalities*. GRAIL 2019, Beyond MIC 2018. Lecture Notes in Computer Science., S. D., Editor. 2018, Springer, Cham.
10. Fornito, A., A. Zalesky, and M. Breakspear, *The connectomics of brain disorders*. Nat Rev Neurosci, 2015. **16**(3): p. 159-72.
11. Badhwar, A., et al., *Resting-state network dysfunction in Alzheimer's disease: A systematic review and meta-analysis*. Alzheimers Dement (Amst), 2017. **8**: p. 73-85.
12. Brier, M.R., J.B. Thomas, and B.M. Ances, *Network dysfunction in Alzheimer's disease: refining the disconnection hypothesis*. Brain Connect, 2014. **4**(5): p. 299-311.
13. Contreras, J.A., et al., *Cognitive complaints in older adults at risk for Alzheimer's disease are associated with altered resting-state networks*. Alzheimers Dement (Amst), 2017. **6**: p. 40-49.
14. Finn, E.S., et al., *Can brain state be manipulated to emphasize individual differences in functional connectivity?* Neuroimage, 2017. **160**: p. 140-151.
15. Finn, E.S., et al., *Functional connectome fingerprinting: identifying individuals using patterns of brain connectivity*. Nat Neurosci, 2015. **18**(11): p. 1664-71.
16. Shen, X., et al., *Using connectome-based predictive modeling to predict individual behavior from brain connectivity*. Nat Protoc, 2017. **12**(3): p. 506-518.
17. Scheinost, D., et al., *Ten simple rules for predictive modeling of individual differences in neuroimaging*. Neuroimage, 2019. **193**: p. 35-45.
18. Yoo, K., et al., *Connectome-based predictive modeling of attention: Comparing different functional connectivity features and prediction methods across datasets*. Neuroimage, 2018. **167**: p. 11-22.
19. Cloutier, S., et al., *Patterns of Cognitive Decline Prior to Dementia in Persons with Mild Cognitive Impairment*. J Alzheimers Dis, 2015. **47**(4): p. 901-13.
20. Aggarwal, N.T., et al., *Mild cognitive impairment in different functional domains and incident Alzheimer's disease*. J Neurol Neurosurg Psychiatry, 2005. **76**(11): p. 1479-84.
21. Zhao, Q., et al., *Cognitive decline in patients with Alzheimer's disease and its related factors in a memory clinic setting, Shanghai, China*. PLoS One, 2014. **9**(4): p. e95755.
22. Lambon Ralph, M.A., et al., *Homogeneity and heterogeneity in mild cognitive impairment and Alzheimer's disease: a cross-sectional and longitudinal study of 55 cases*. Brain, 2003. **126**(Pt 11): p. 2350-62.
23. Zhan, Y., et al., *Network-Based Statistic Show Aberrant Functional Connectivity in Alzheimer's Disease*. IEEE Journal of Selected Topics in Signal Processing, 2016. **10**(7): p. 1182-1188.
24. Wook Yoo, S., et al., *A Network Flow-based Analysis of Cognitive Reserve in Normal Ageing and Alzheimer's Disease*. Sci Rep, 2015. **5**: p. 10057.
25. Buckner, R.L., et al., *Cortical hubs revealed by intrinsic functional connectivity: mapping, assessment of stability, and relation to Alzheimer's disease*. J Neurosci, 2009. **29**(6): p. 1860-73.

26. Buckner, R.L., et al., *Molecular, structural, and functional characterization of Alzheimer's disease: evidence for a relationship between default activity, amyloid, and memory*. J Neurosci, 2005. **25**(34): p. 7709-17.
27. Seeley, W.W., et al., *Neurodegenerative diseases target large-scale human brain networks*. Neuron, 2009. **62**(1): p. 42-52.
28. Vogel, J.W., et al., *Brain properties predict proximity to symptom onset in sporadic Alzheimer's disease*. Brain, 2018. **141**(6): p. 1871-1883.
29. Lin, Q., et al., *Resting-State Functional Connectivity Predicts Cognitive Impairment Related to Alzheimer's Disease*. Front Aging Neurosci, 2018. **10**: p. 94.
30. Duchek, J.M., et al., *Relationship between Stroop performance and resting state functional connectivity in cognitively normal older adults*. Neuropsychology, 2013. **27**(5): p. 516-28.
31. Amico, E., et al., *Mapping the functional connectome traits of levels of consciousness*. Neuroimage, 2017. **148**: p. 201-211.
32. Power, J.D., et al., *Spurious but systematic correlations in functional connectivity MRI networks arise from subject motion*. Neuroimage, 2012. **59**(3): p. 2142-54.
33. Power, J.D., et al., *Methods to detect, characterize, and remove motion artifact in resting state fMRI*. NeuroImage, 2014. **84**: p. 320-341.
34. Shen, X., et al., *Groupwise whole-brain parcellation from resting-state fMRI data for network node identification*. Neuroimage, 2013. **82**: p. 403-15.
35. Mawlawi, O., et al., *Imaging Human Mesolimbic Dopamine Transmission With Positron Emission Tomography: I. Accuracy and Precision of D2 Receptor Parameter Measurements in Ventral Striatum*. Journal of Cerebral Blood Flow and Metabolism, 2001. **21**: p. 1034-1057.
36. Yeo, B.T., et al., *Estimates of segregation and overlap of functional connectivity networks in the human cerebral cortex*. Neuroimage, 2014. **88**: p. 212-27.
37. Efron, B., *Bootstrap methods: another look at the jackknife*. Annals of Statistics, 1979. **7**(1): p. 1-26.
38. Mingrui, X., J. Wang, and Y. He, *BrainNet Viewer: A Network Visualization Tool for Human Brain Connectomics*. Plos One, 2013. **8**(7).
39. *Correction for Dixon et al., Heterogeneity within the frontoparietal control network and its relationship to the default and dorsal attention networks*. Proc Natl Acad Sci U S A, 2018. **115**(13): p. E3068.
40. Brier, M.R., et al., *Loss of intranetwork and internetwork resting state functional connections with Alzheimer's disease progression*. J Neurosci, 2012. **32**(26): p. 8890-9.
41. Cattaneo, Z., et al., *Contrasting early visual cortical activation states causally involved in visual imagery and short-term memory*. Eur J Neurosci, 2009. **30**(7): p. 1393-400.
42. Pearson, J., et al., *Mental Imagery: Functional Mechanisms and Clinical Applications*. Trends Cogn Sci, 2015. **19**(10): p. 590-602.
43. Jones, D.T., et al., *Cascading network failure across the Alzheimer's disease spectrum*. Brain, 2016. **139**(Pt 2): p. 547-62.
44. Zhou, J., et al., *Divergent network connectivity changes in behavioural variant frontotemporal dementia and Alzheimer's disease*. Brain, 2010. **133**(Pt 5): p. 1352-67.
45. Garces, P., et al., *The Default Mode Network is functionally and structurally disrupted in amnesic mild cognitive impairment - a bimodal MEG-DTI study*. Neuroimage Clin, 2014. **6**: p. 214-21.
46. Sperling, R.A., et al., *Amyloid deposition is associated with impaired default network function in older persons without dementia*. Neuron, 2009. **63**(2): p. 178-88.
47. Wang, L., et al., *Cerebrospinal fluid Abeta42, phosphorylated Tau181, and resting-state functional connectivity*. JAMA Neurol, 2013. **70**(10): p. 1242-8.
48. Hedden, T., et al., *Disruption of functional connectivity in clinically normal older adults harboring amyloid burden*. J Neurosci, 2009. **29**(40): p. 12686-94.
49. Cope, T.E., et al., *Tau burden and the functional connectome in Alzheimer's disease and progressive supranuclear palsy*. Brain, 2018. **141**(2): p. 550-567.

**Supplementary Figures**

**Montreal Cognitive Test**

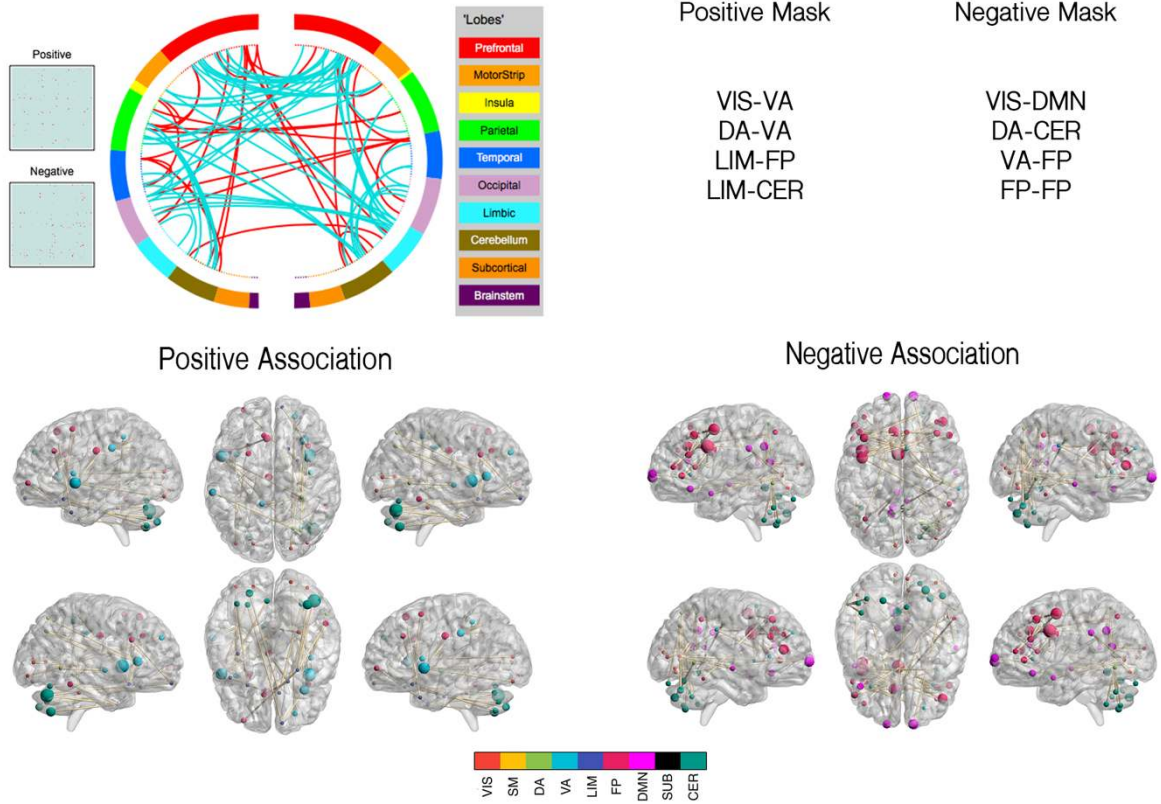


**Figure S1:** Over represented edges (binomial test,  $\alpha = 0.01$ ) for the Montreal Cognitive Association Test (MOCA). (Top Left) Cluster gram delineating anatomical locations and sign of over represented edges (blue – positively associated edges, red – negatively associated edges). (Top Right) RSNs that are over represented beyond change. (Bottom) Glass brain plot of over represented edges where nodes are weighted by degree and colored according to RSN. Positively associated edges (left) and negatively associated edges (right) are visualized separately.

## Auditory Verbal Learning Immediate Recall

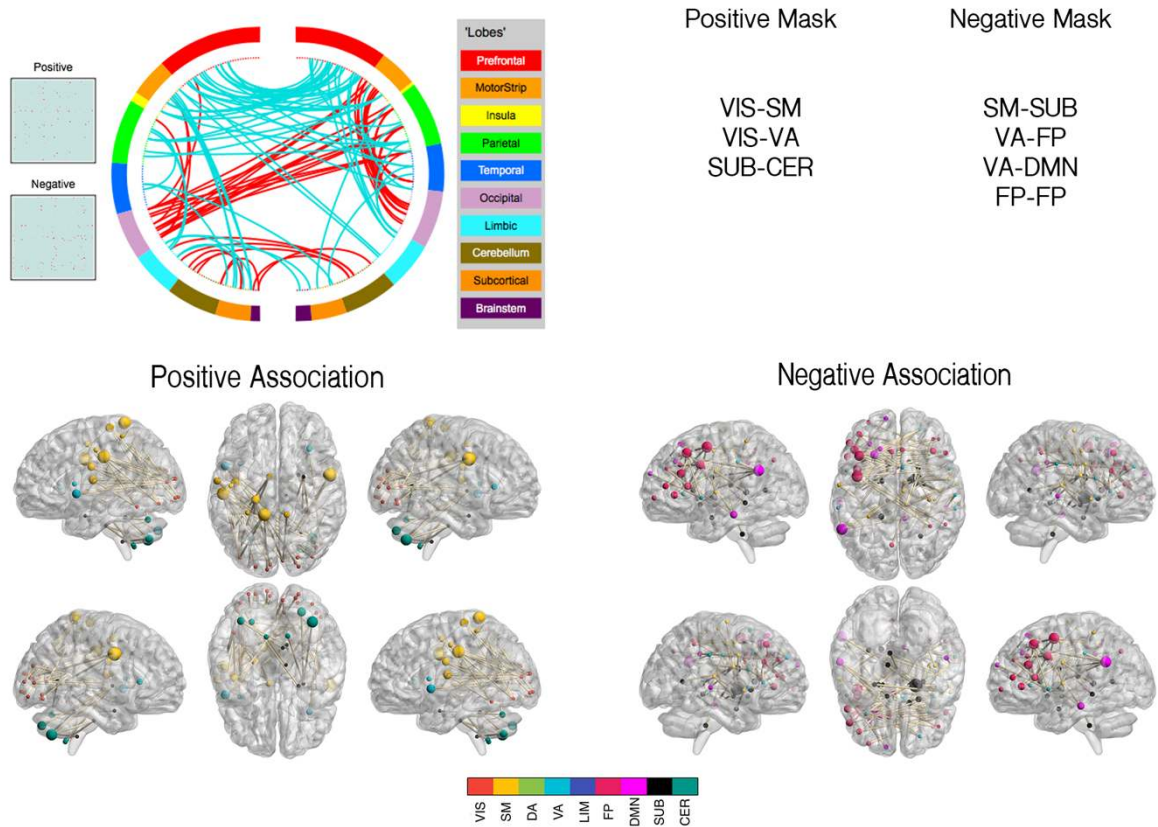


**Figure S2:** Over represented edges (binomial test,  $\alpha = 0.01$ ) for the AVLT Immediate Recall test. (Top Left) Cluster graph delineating anatomical locations and sign of over represented edges (blue – positively associated edges, red – negatively associated edges). (Top Right) RSNs that are over represented beyond change. (Bottom) Glass brain plot of over represented edges where nodes are weighted by degree and colored according to RSN. Positively associated edges (left) and negatively associated edges (right) are visualized separately.

### Auditory Verbal Learning Delayed Recall

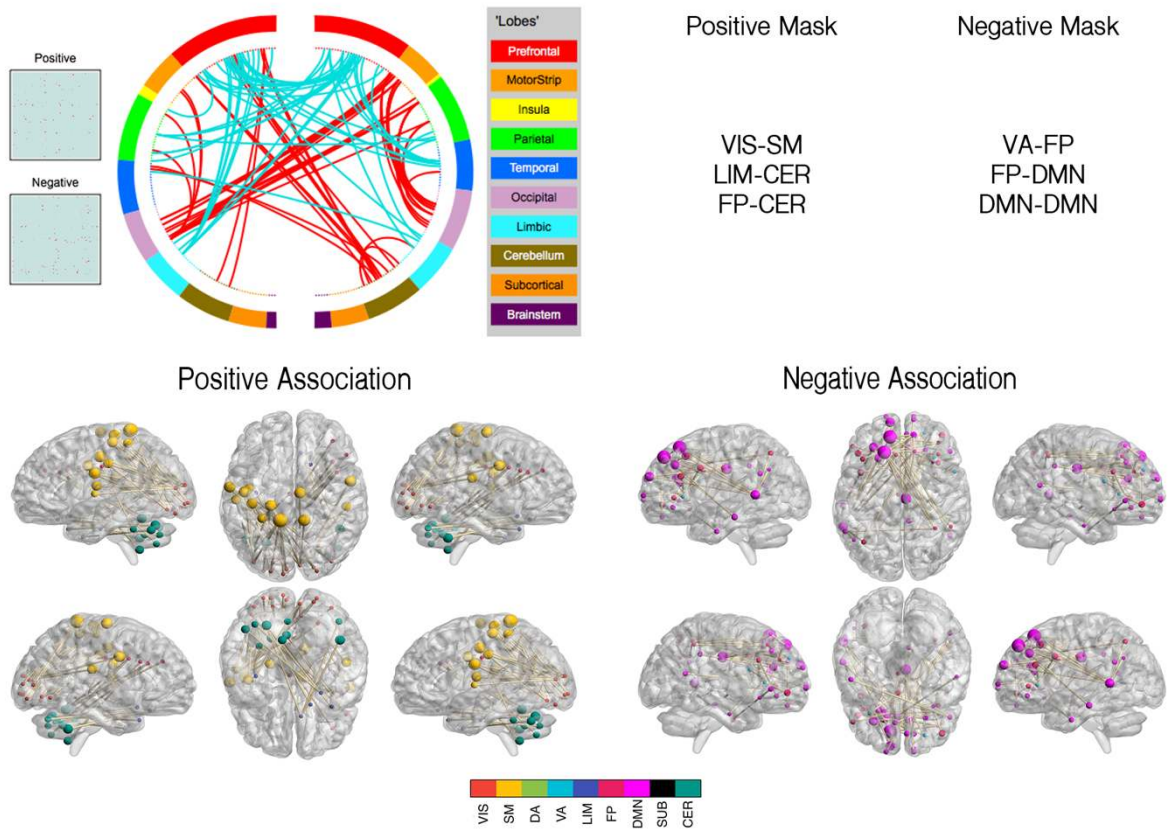


**Figure S3:** Over represented edges (binomial test,  $\alpha = 0.01$ ) for the AVLT Delayed Recall test. (Top Left) Cluster gram delineating anatomical locations and sign of over represented edges (blue – positively associated edges, red – negatively associated edges). (Top Right) RSNs that are over represented beyond change. (Bottom) Glass brain plot of over represented edges where nodes are weighted by degree and colored according to RSN. Positively associated edges (left) and negatively associated edges (right) are visualized separately.

## Boston Naming

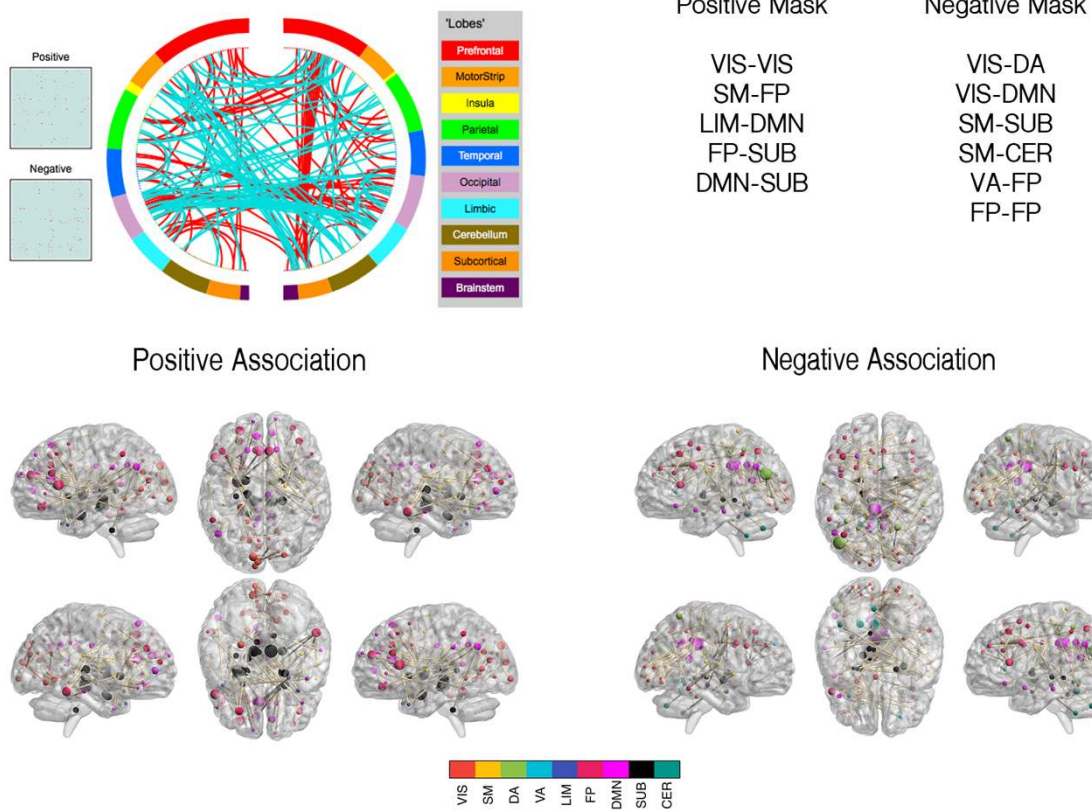


**Figure S4.** Over represented edges (binomial test,  $\alpha = 0.01$ ) for the Boston Naming Test. (Top Left) Cluster gram delineating anatomical locations and sign of over represented edges (blue – positively associated edges, red – negatively associated edges). (Top Right) RSNs that are over represented beyond change. (Bottom) Glass brain plot of over represented edges where nodes are weighted by degree and colored according to RSN. Positively associated edges (left) and negatively associated edges (right) are visualized separately.

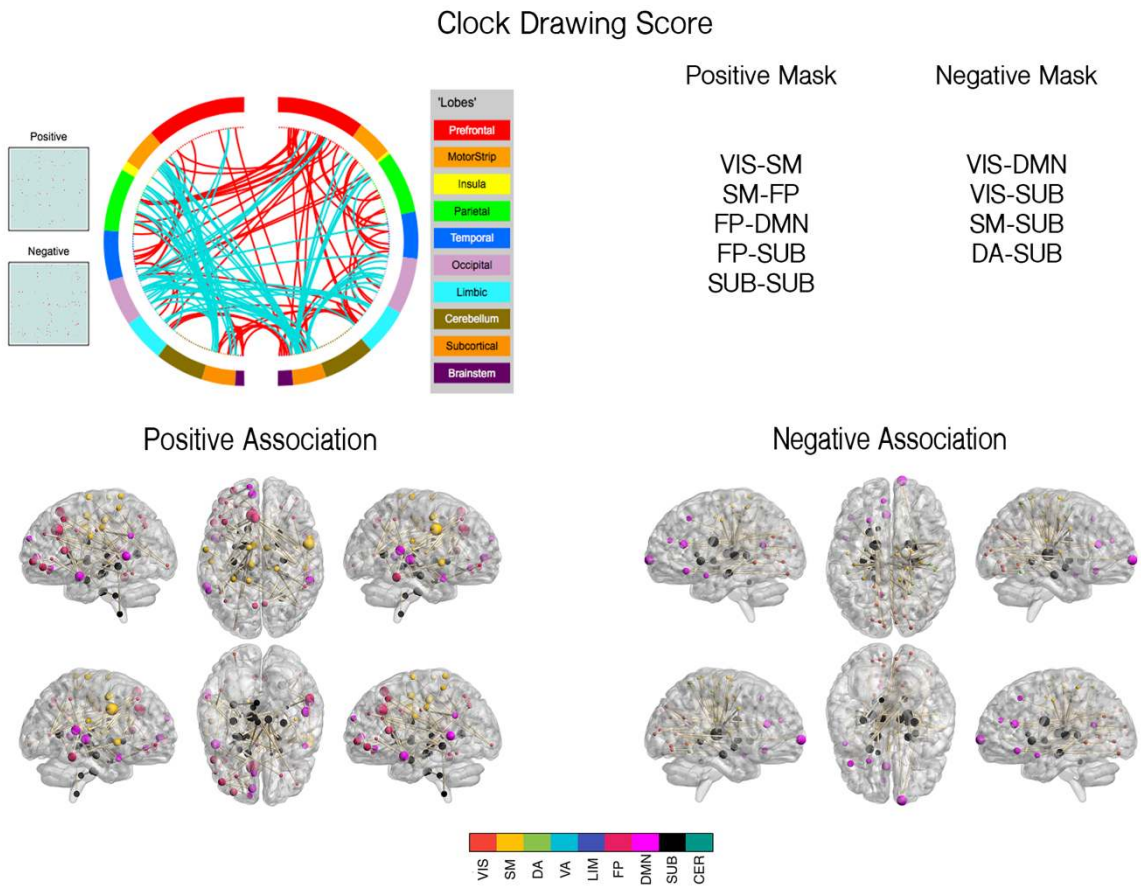


**Figure S5.** Over represented edges (binomial test,  $\alpha = 0.01$ ) for the Clock Drawing Test. (Top Left) Cluster gram delineating anatomical locations and sign of over represented edges (blue – positively associated edges, red – negatively associated edges). (Top Right) RSNs that are over represented beyond change. (Bottom) Glass brain plot of over represented edges where nodes are weighted by degree and colored according to RSN. Positively associated edges (left) and negatively associated edges (right) are visualized separately.

## Trails B Score

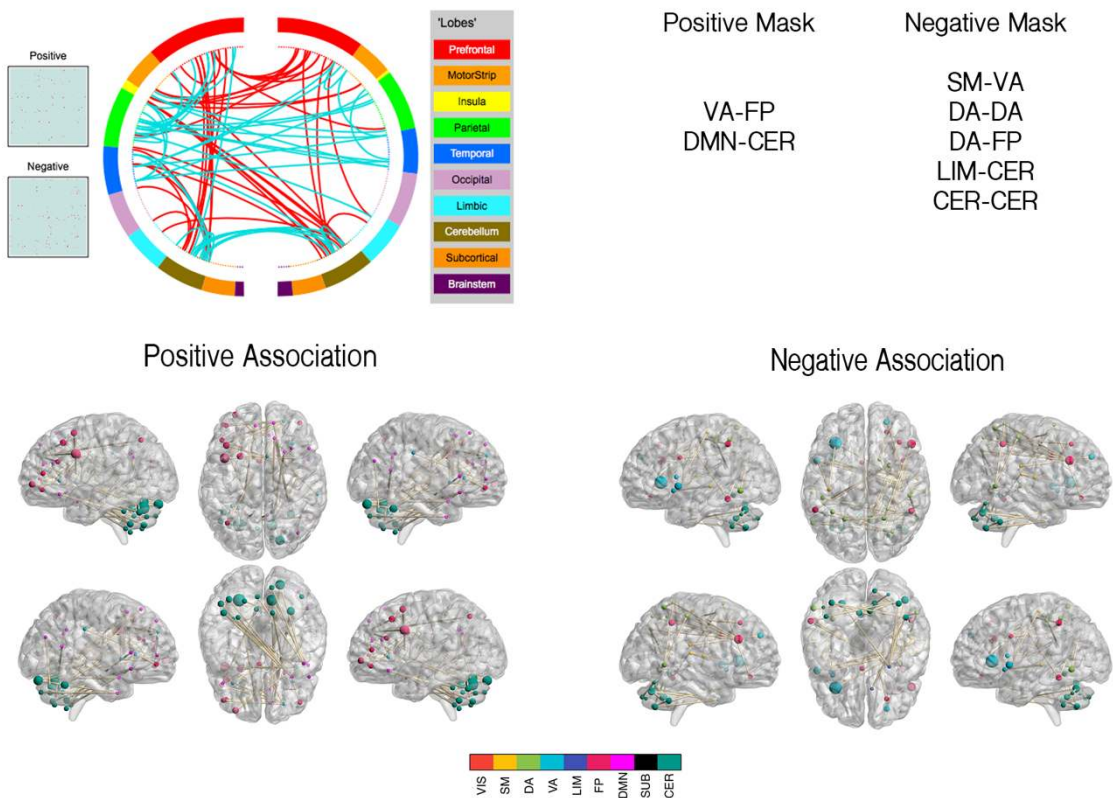


**Figure S6:** Over represented edges (binomial test,  $\alpha = 0.01$ ) for the Trail Making B test. (Top Left) Cluster gram delineating anatomical locations and sign of over represented edges (blue – positively associated edges, red – negatively associated edges). (Top Right) RSNs that are over represented beyond change. (Bottom) Glass brain plot of over represented edges where nodes are weighted by degree and colored according to RSN. Positively associated edges (left) and negatively associated edges (right) are visualized separately.